A Direct Approach to Zn^{2+} Pre-Intercalated V_2O_5 Cathodes with Superior Electrochemical Performance for Aqueous Zinc-Ion Batteries

Mayank K. Singh[a], Sarvesh Aware[a], Pranjal Jaiswal[a], Sheetal Gupta[a], Khushwant Singh[a], Neha Chaudhary[a], Govind Kumar Maurya[a] and Dhirendra K. Rai[a,b]*

[a]*Sustainable Energy and Environmental Materials (SEEM) Lab, Department of Metallurgical Engineering and Materials Science, Indian Institute of Technology Indore, Simrol, Indore 453552, India.*

[b]*Microstructure and Texture Engineering Lab, Department of Metallurgical Engineering and Materials Science, Indian Institute of Technology Indore, Simrol, Indore 453552, India.*

*Corresponding author: Dr. Dhirendra K. Rai, E-mail: *dkrai@iiti.ac.in; Tel: +91 731 660 3278*

List of Content

1. Chemicals

Vanadium Pentoxide (V_2O_5)-99%, Phosphoric Acid (H_3PO_2 were purchased from SRL Chemical. Zinc Strip was purchased from BATSOL India. Throughout the synthesis, deionized water (Millipore DI water, 18.2 MΩcm-1) was used.

2. Physiochemical Characterization: Powder X-ray diffraction (PXRD) was performed on a Bruker AXA D8 Advance diffractometer using monochromatic Cu Kα radiation (λ = 1.54 Å) over a 2θ range of 5–80° with a step size of 0.02° min^{-1}. Morphological and elemental analyses were conducted via field-emission scanning electron microscopy (FE-SEM, JEOL 7610F Plus) equipped with energy-dispersive X-ray spectroscopy (EDS). Fourier-transform infrared (FTIR) spectra were recorded on a Bruker Tensor 27 spectrometer in the 400–4000 cm^{-1} range. X-ray photoelectron spectroscopy (XPS) was carried out using a Shimadzu spectrometer with an Al Kα source (1486.7 eV).

3. Electrochemical measurements: The electrochemical properties of the electrodes were tested using Autolab 204 potentiostat and NEWARE battery test system to carry out the electrochemical performance of the electrode.

4. Assembly of coin cell: Coin cells were assembled to evaluate the electrochemical performance of both pristine V_2O_5 and Zn-intercalated $V_2O_5 \cdot nH_2O$ ($Zn_xV_2O_5 \cdot nH_2O$) cathodes. The cathode slurry was prepared by mixing the active material (either V_2O_5 or $Zn_xV_2O_5 \cdot nH_2O$), [1]polyvinylidene fluoride (PVDF), and Super P carbon in a weight ratio of 8:1:1 using N-methyl-2-pyrrolidone (NMP) as the solvent. The resulting slurry was uniformly coated onto stainless steel foil and dried to form the cathode electrode. For both cell types, zinc foil was used as the anode, and 3 M $Zn(CF_3SO_3)_2$ served as the electrolyte. The cells were assembled in a CR2032 coin cell configuration with a standard separator under ambient conditions. The fabrication process was identical for both V_2O_5//Zn and $Zn_xV_2O_5 \cdot nH_2O$//Zn cells, differing only in the choice of active cathode material.

5. Computational Details: First-principles density functional theory (DFT) calculations were performed using the Vienna *ab initio* Simulation Package (VASP). [1,2]The generalized gradient approximation (GGA) with projector-augmented wave (PAW) potentials was employed for both electronic and structural optimizations. A plane-wave cutoff energy of 450 eV and an energy convergence criterion of 10^{-4} eV were applied. Geometry optimizations were carried out with a force convergence threshold of 0.03 eV $Å^{-1}$ using a 4 × 4 × 1 Monkhorst–Pack K-point grid. For electronic structure calculations, the K-point mesh was refined to 10 × 10 × 1.

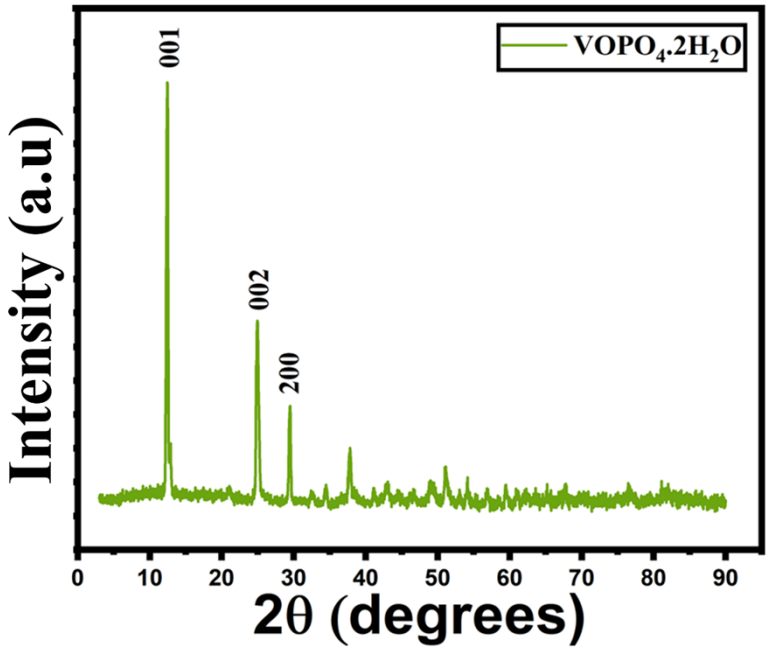

Fig. S1 XRD pattern of $VOPO_4.2H_2O$

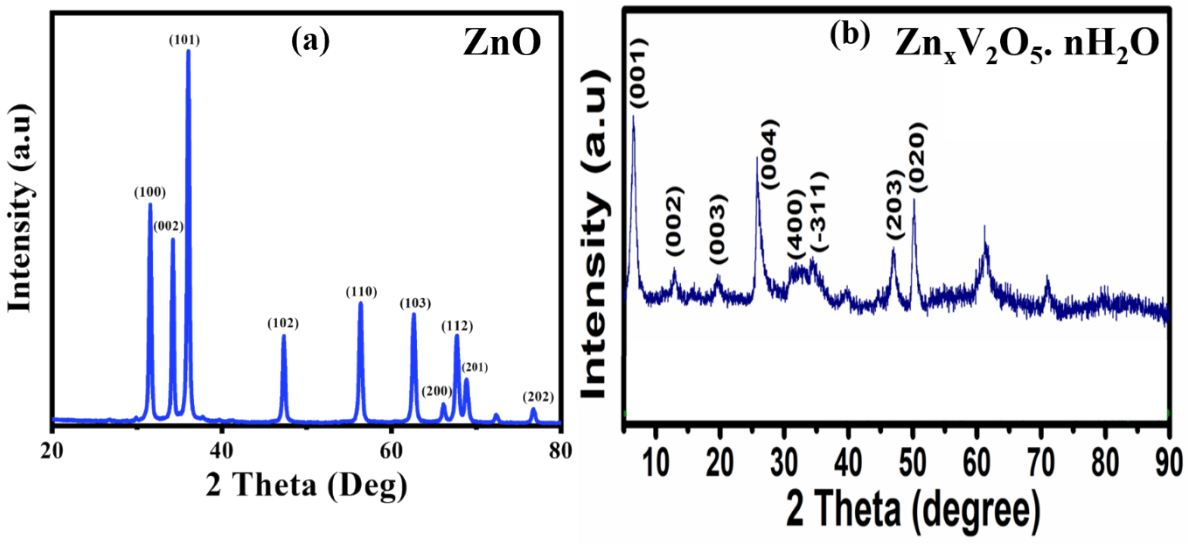

Fig. S2. XRD pattern of synthesized pure (a) ZnO and (b) $Zn_xV_2O_5.nH_2O$.

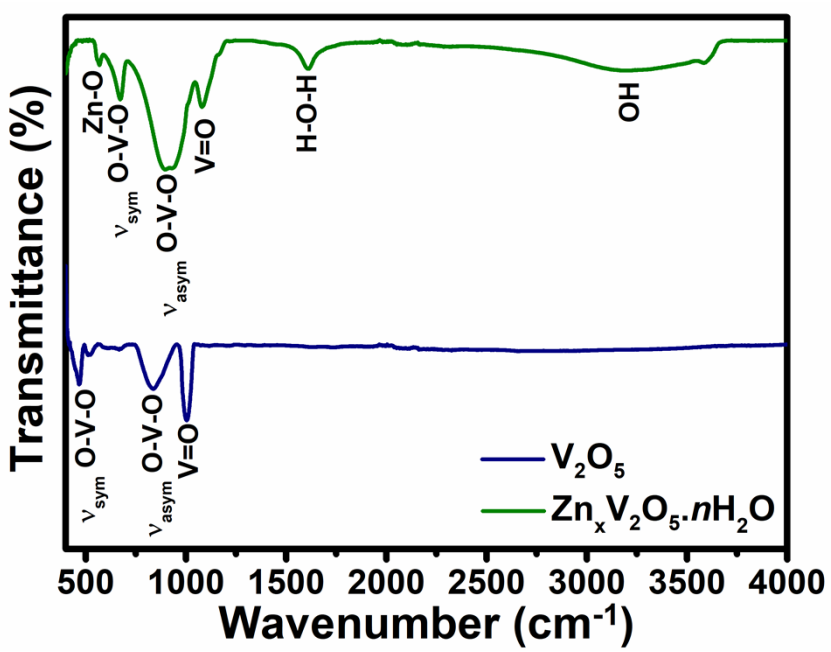

Fig. S3 FTIR spectra of V_2O_5 and $Zn_xV_2O_5{\cdot}nH_2O$

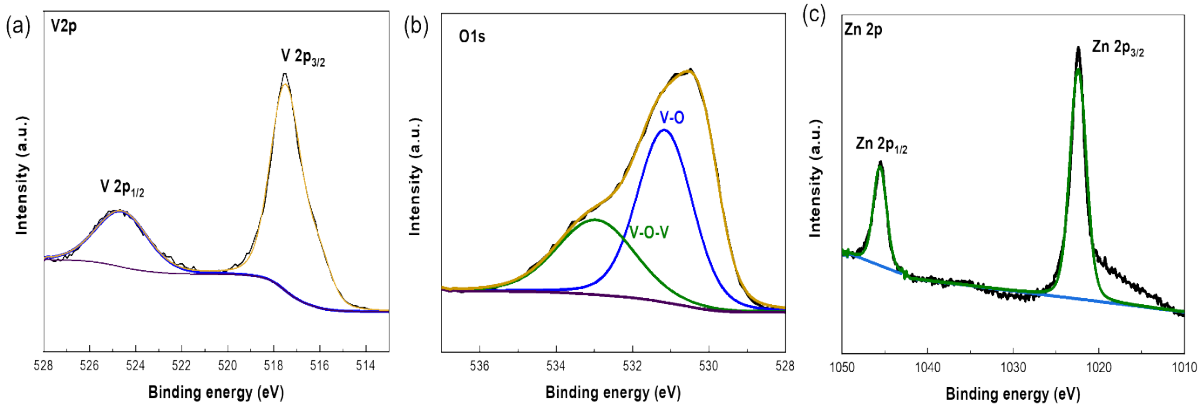

Fig. S4 XPS high-resolution spectra of (a) V 2p, (b) O 1s, and (c) Zn 2p of $Zn_xV_2O_5{\cdot}nH_2O$

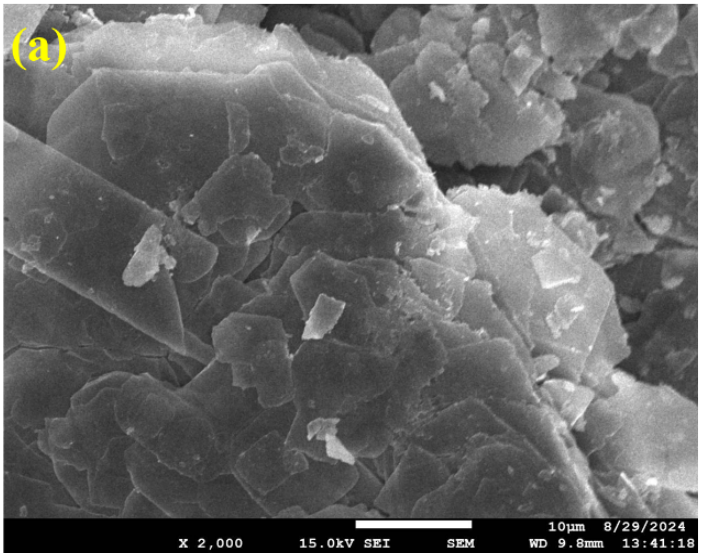

Fig. S5 FESEM of $VOPO_4.2H_2O$

Dunn's Analysis: To quantify the contributions of surface-controlled and diffusion-controlled processes to the overall capacitance, Dunn's method was employed. This approach expresses the cyclic voltammetric (CV) current response at a given potential as a function of the scan rate (v), considering both capacitive and diffusion-controlled mechanisms, as described by the equation:

$$\mathbf{i(v) = k_1 v + k_2 v^{1/2}} \quad (1)$$

where i(v) is the current at a fixed potential and k_1 and k_2 are constant values for the surface-controlled and diffusion-controlled processes, respectively.

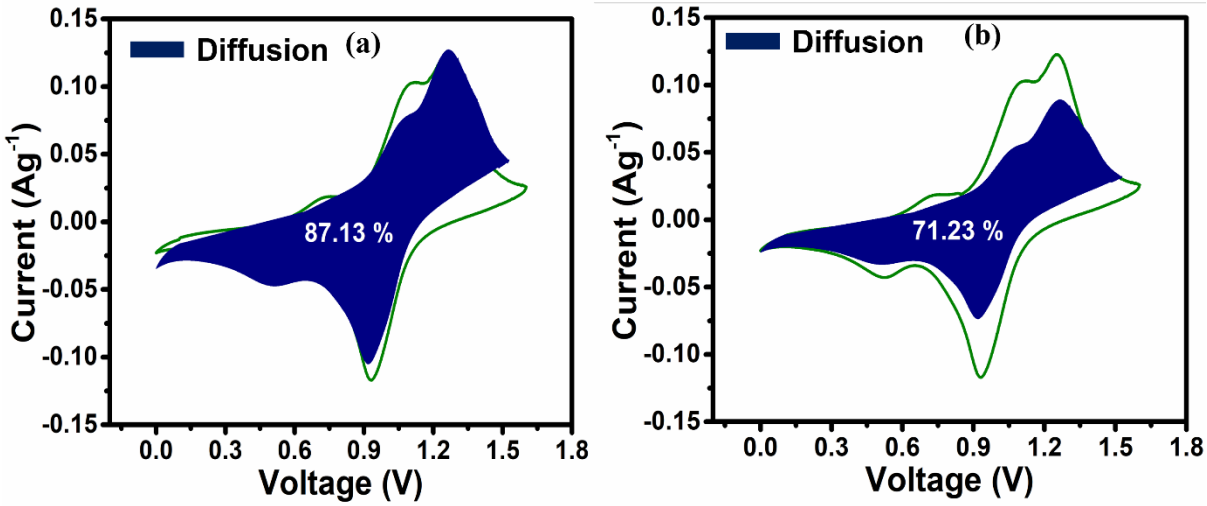

Fig. S6 Contributions of surface and diffusion-controlled processes to the overall CV profile of $Zn_xV_2O_5{\cdot}nH_2O$ at 5 mVs^{-1} and 50 mVs^{-1}.

Evaluation of contribution of H^+ intercalation in charge storage: The electrochemical behavior of Zn^{2+} intercalation in V_2O_5 must be considered in the context of potential H^+ co-intercalation, particularly given the aqueous electrolyte environment and the inherent proton conductivity of hydrated vanadium oxides ($V_2O_5 \cdot nH_2O$). The smaller ionic radius and higher mobility of H^+ ions facilitate their preferential insertion into interlayer galleries, especially during initial discharge stages, where they participate in charge compensation during the V^{5+}/V^{4+} redox process. This hypothesis is supported by both the observed 0.3 pH unit decrease in 3 M $Zn(CF_3SO_3)_2$ electrolyte after 20 cycles. Further, control experiments using Nafion proton-exchange membrane separator exhibited dramatically reduced Cyclic voltammetry area and maximum current with reduced capacity (34.6 mAh/g), confirming that H^+ transport contribution is minimal.[8]

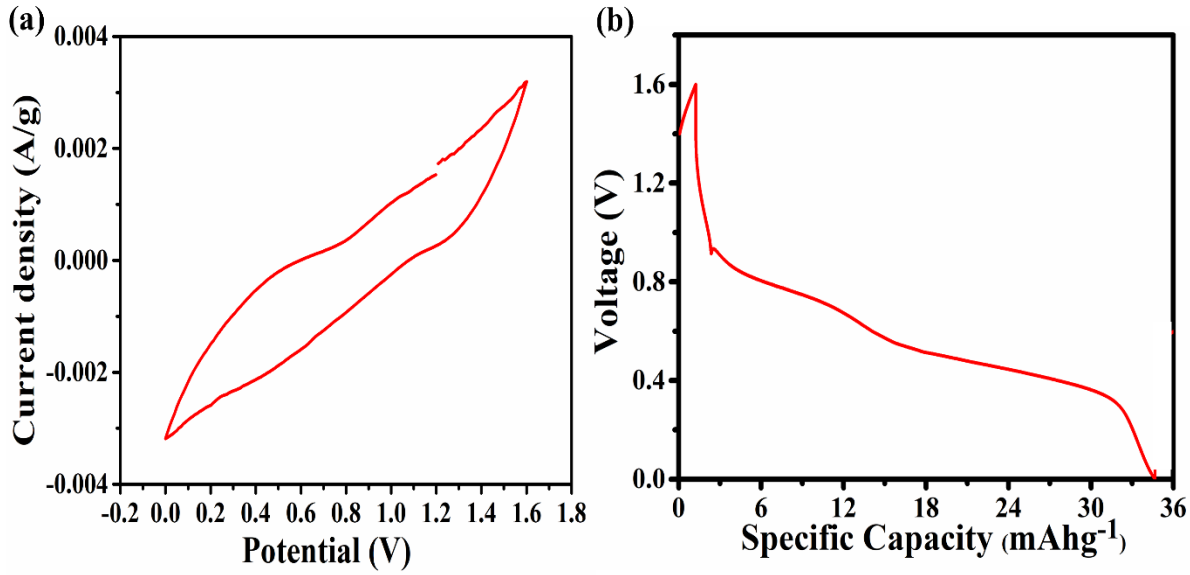

Fig. S7 Electrochemical characterization of $Zn_xV_2O_5 \cdot nH_2O$ using Nafion proton-exchange membrane separator. (a) Cyclic voltammetry curves (10 mV/s) show complete suppression of redox peaks compared to standard separator (b) Galvanostatic charge-discharge profiles (0.1 A/g) exhibit severely limited capacity (34.6 mAh/g). These control experiments suggest that the contribution of H^+ intercalation in charge storage is very low compared to the total charge, and Zn^{2+} intercalation is the primary charge storage mechanism.

Performance sensitivity towards type of Zn strip used during hydrothermal process: The quality of zinc sources significantly impacts both Zn^{2+} intercalation efficiency and the reproducibility of hydrothermal synthesis, as metallic zinc serves dual roles as both reducing agent and Zn^{2+} source. Surface oxides (e.g., $ZnO/Zn(OH)_2$) and metallic impurities (Fe, Pb, Cu) were found to alter dissolution kinetics and vanadium redox states, with control experiments demonstrating a capacity reduction (280 vs. 324 mAh g^{-1}) when using commercial zinc alloy versus high-purity foil (99.99%). These results, underscore the necessity of employing rigorously cleaned (acid-etched/polished), high-purity zinc to ensure consistent intercalation behaviour and optimal electrochemical performance.

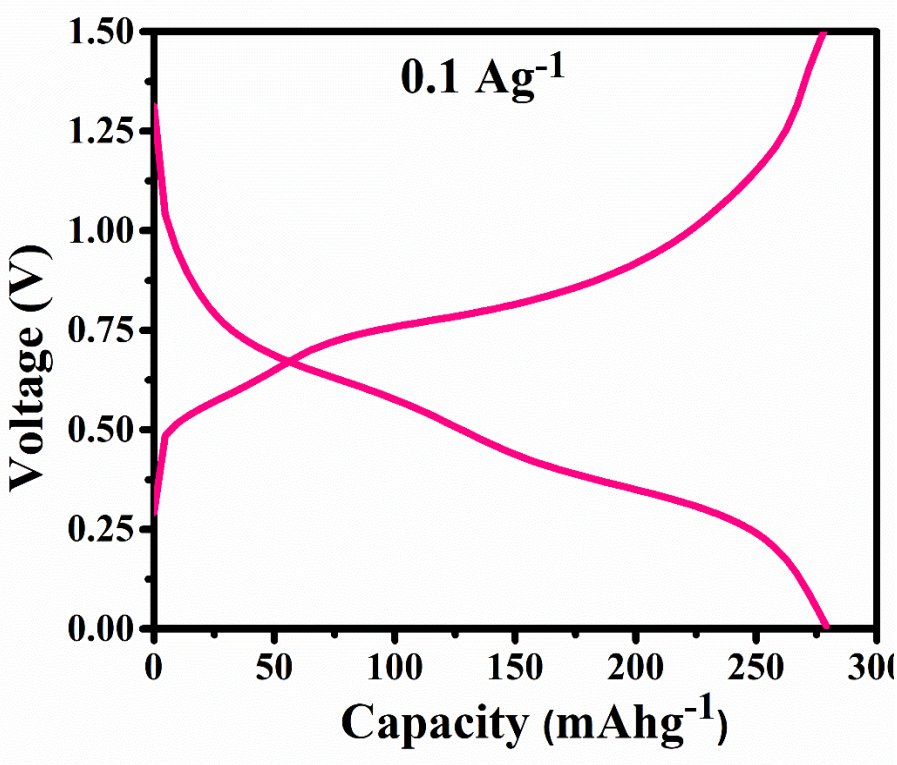

Fig. S8 Galvanostatic charge-discharge (GCD) profiles of $Zn_xV_2O_5{\cdot}nH_2O$ synthesized using a commercial zinc alloy strip (3 M $Zn(CF_3SO_3)_2$ electrolyte, 50 mA g^{-1} current density). The reduced specific capacity (280 mAh g^1 vs. 324 mAh g^1 for high-purity Zn foil) highlights the detrimental effects of alloy-derived impurities on Zn^{2+} intercalation kinetics and redox stability.

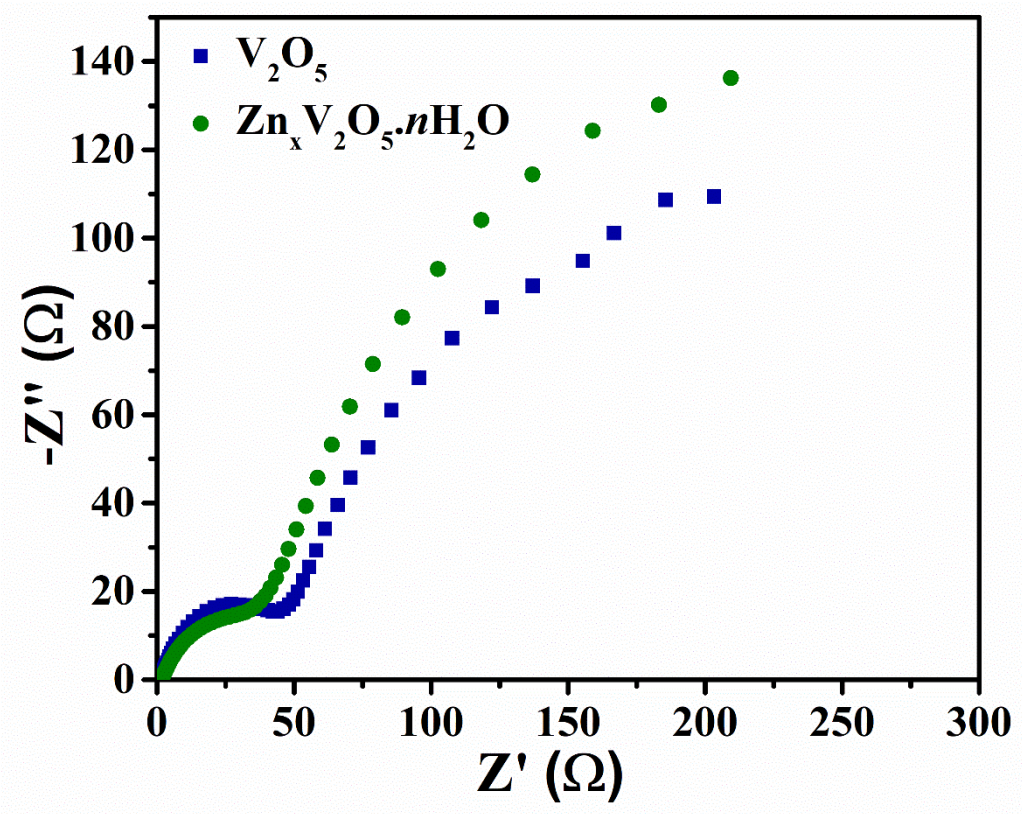

Fig. S9 EIS spectra of V_2O_5 and $Zn_xV_2O_5 \cdot nH_2O$.

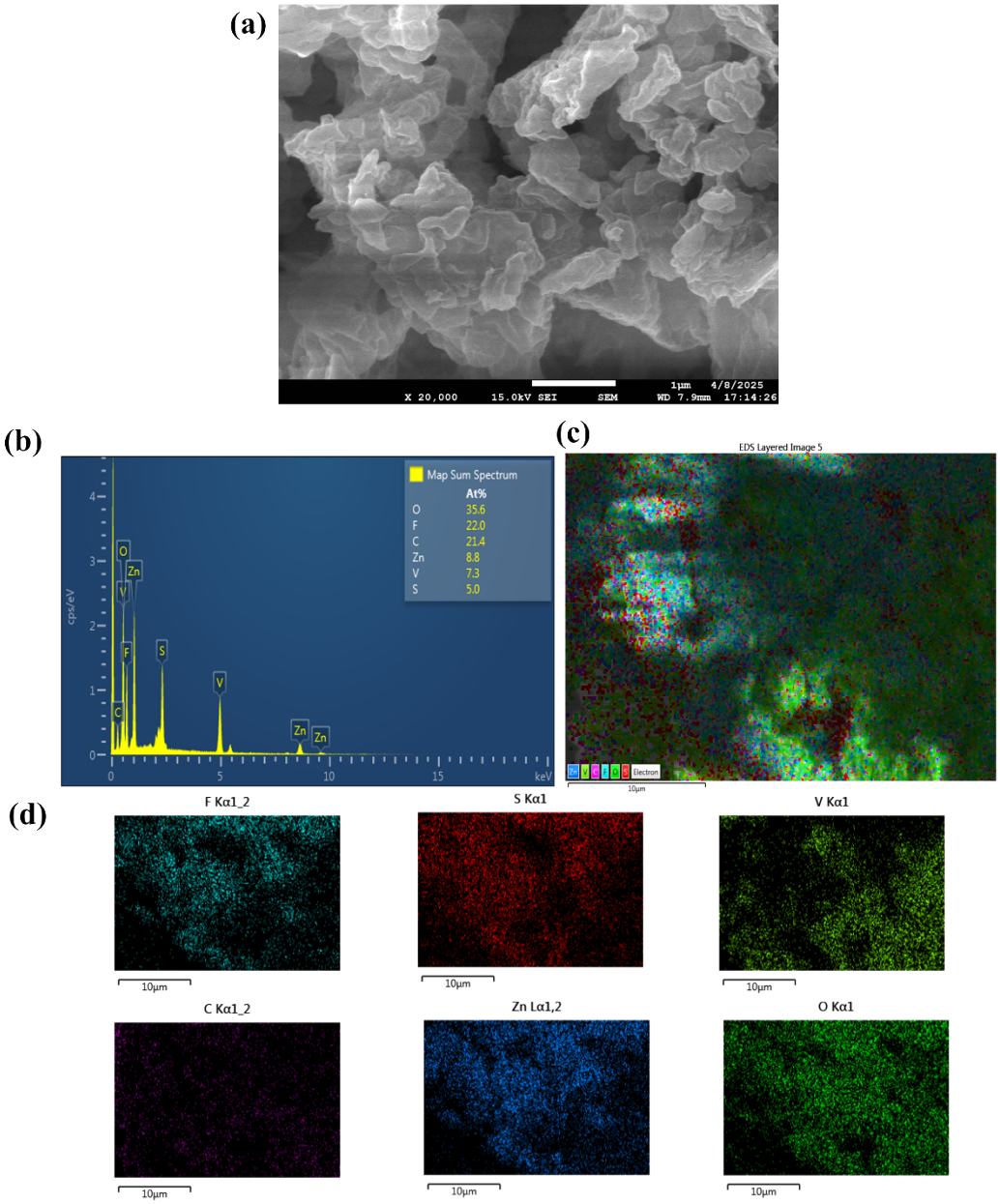

Fig. S10 (a,b,c,d) FESEM, EDX and elemental mapping of $Zn_xV_2O_5{\cdot}nH_2O$ after cycling.

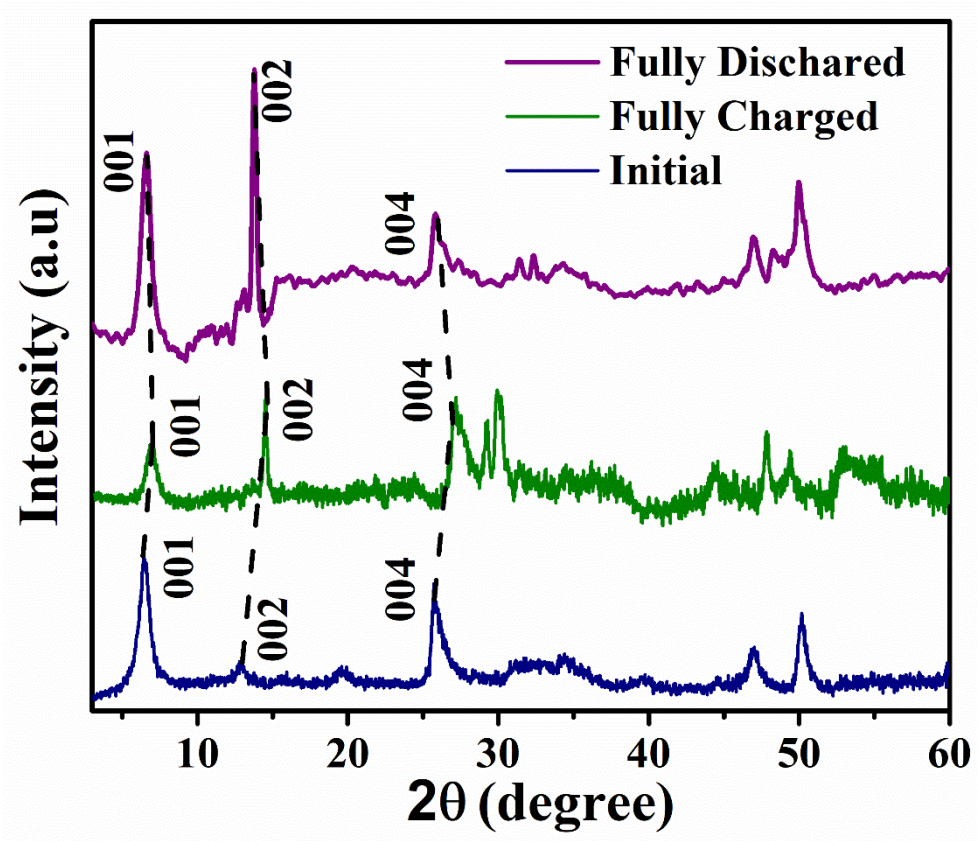

Fig. S11 XRD spectra of $Zn_xV_2O_5{\cdot}nH_2O$ at various charging and discharging steps.

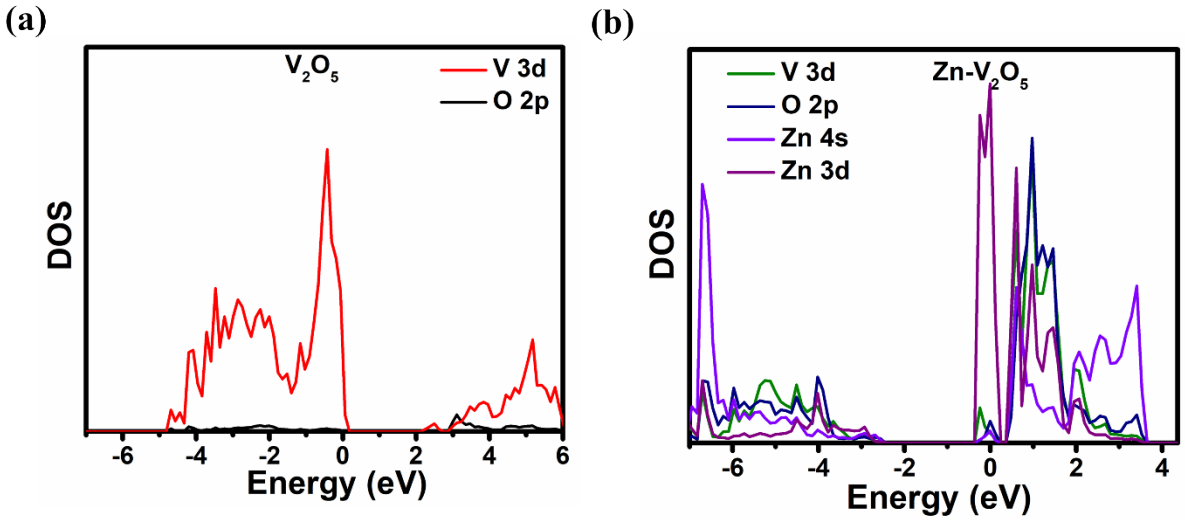

Fig. S12 (a, b) PDOS of V_2O_5 and $Zn_xV_2O_5 \cdot nH_2O$.($Zn_xV_2O_5 \cdot nH_2O$ featuring significant enhanced Zinc 3d contribution near Fermi level).

Table S1. Comparison Table of reported pre-intercalated Zn^{2+} in V_2O_5

S. No	Cathode	Method	Specific Capacity	Retention/Cycle	Energy Density ($0.1\ Ag^{-1}$)	Capacity Retention (%) ($0.1\ Ag^{-1}$- $5\ Ag^{-1}$)	Ref
1	$Zn_{0.25}V_2O_5{\cdot}nH_2O$	Microwave Hydrothermal method	300 mAh g^{-1}	80%/1000	$450Wh^{-1}$	-----	3
2	$Zn_xV_2O_5{\cdot}nH_2O$	Hydrothermal method	295 mAh g^{-1}	48%/100	----	80% ($0.1\ Ag^{-1}$- $2Ag^{-1}$)	4
3	$Zn_{0.3}V_2O_5{\cdot}1.5H_2O$	Hydrothermal method	426.3 mAh g^{-1}	96%/20000	274 Wh kg^{-1}	78.4 % ($0.1\ Ag^{-1}$- $5\ Ag^{-1}$)	5
4	ZVO	Microwave Hydrothermal method	355 mAh g^{-1}	84%/500	------	50% ($0.1\ Ag^{-1}$- $2Ag^{-1}$)	6
5	Zn-$V_2O_5{\cdot}nH_2O$	Sol-gel/Freez Drying	140 mAh g^{-1}	137%/100	-------	64% ($0.1\ Ag^{-1}$- $1Ag^{-1}$)	7
6	$Zn_xV_2O_5{\cdot}nH_2O$	Zinc Strip in Hydrothermal method	324 mAh g^{-1}	97.3%/5000	231 Wh kg^{-1}	85 % ($0.1\ Ag^{-1}$- $5Ag^{-1}$)	**This Work**

References

1 G. Kresse and J. Furthmüller, *Computational Materials Science*, 1996, **6**, 15–50.

2 G. Kresse and J. Hafner, *Phys. Rev. B*, 1994, **49**, 14251–14269.

3 D. Kundu, B. D. Adams, V. Duffort, S. H. Vajargah and L. F. Nazar, *Nat Energy*, 2016, **1**, 16119.

4 Y. Fan, X. Yu, Z. Feng, M. Hu and Y. Zhang, *Molecules*, 2022, **27**, 5387.

5 L. Wang, K.-W. Huang, J. Chen and J. Zheng, *Sci. Adv.*, 2019, **5**, eaax4279.

6 X. Liu, X. Dong and S. Passerini, *Journal of Power Sources*, 2024, **623**, 235401.

7 Y. Li, W. Xu, T. Sun and J. Yao, *Journal of Electroanalytical Chemistry*, 2023, **937**, 117416.

8. Zhang, N., Jia, M., Dong, Y., Wang, Y., Xu, J., Liu, Y., Jiao, L., & Cheng, F. 2019, *Advanced Functional Materials*, **29**, 1906346.